






Performance of NOMA-Based Dual-Hop Hybrid Powerline-Wireless Communication Systems

Ahmed Samir , *Student Member, IEEE*, Mohamed Elsayed , *Student Member, IEEE*,
Ahmad A. Aziz El-Banna , *Member, IEEE*, Kaishun Wu , *Senior Member, IEEE*,
and Basem M. ElHalawany , *Senior Member, IEEE*

Abstract—The mixture of wireless and power line communications (PLC) is vital for implementing new applications in smart grid and vehicular communications. In this work, we investigate the performance of non-orthogonal multiple access (NOMA) based dual-hop hybrid communication systems with decode-and-forward relay. The wireless channel is characterized by Nakagami- m fading under an additive white Gaussian noise (AWGN), while the PLC channels are characterized by Log-normal distribution with Bernoulli Gaussian noise including both background and impulsive noise components. New closed-form expressions for the outage probability, the asymptotic outage probability and ergodic capacity are derived and verified via extensive representative simulations. For more insights on the outage performance, we analyze the diversity order. Additionally, we proposed a power allocation optimization technique to achieve an outage-optimal performance. The results show that the system outage probability improves as the impulsive noise index and the arrival probability of the impulsive component of the PLC additive noise decrease, while their effect is negligible on the ergodic capacity. Finally, the performance of the proposed system is compared against a benchmark OMA-based system.

Index Terms—Decode and forward relay, ergodic capacity, non-orthogonal multiple access, outage probability, power line communications.

I. INTRODUCTION

TRANSMISSION over different communication channels such as radio frequency (RF), visible light communication (VLC), underwater wireless optical communication (UWOC), and power line communications (PLC) has been investigated under the umbrella of heterogeneous future generations of communication networks such as 5G, Beyond 5G (B5G), and 6G [1]–[3]. Moreover, the exchange of information through hybrid networks where the transmitter and the receivers use different technologies has recently grabbed attention. Several combinations have been considered in the literature using either

decode-and-forward (DF) or amplify-and-forward (AF) relaying [28] including hybrid PLC/VLC [3], hybrid RF/PLC [4], [5], and hybrid RF/VLC/PLC [6]. VLC is preferred over the indoor RF network as it offers a revolutionary solution for high data rate indoor transmission [7], while the PLC for backhauling has lately grasped attention due to availability at each home [8], [9].

PLC is one of the most vital technology nowadays, as it provides a ready infrastructure for communicating with end-users as it covers huge geographical areas. PLC can cope with new communication demands and the need for fast and easy access to data [10]. The main drawback of PLC is that it wasn't designed as a communication channel, so signals traveling through PLC links suffer from harsh noise, and it is one of the major obstacles in using PLC as a communication channel. The parameters of PLC witness a great fluctuation in their values, especially at high data rates, which makes the channel noise modeling a hard task [11], [12]. Consequently, we must take the impulsive noise (IMN) and background noise (BGN) into our consideration to model the additive noise [13], [14]. IMN statistical features are characterized by Middleton class A distribution [15], while BGN is characterized by the Nakagami- m distribution [16].

Additionally, the RF/PLC system configuration provides a solution for indoor RF signal propagation losses due to penetration of thick walls and metal structures by using indoor PLC ability equipment. On the other hand, the PLC/RF system configuration provides a good connectivity solution between the power companies and the consumers' homes equipment with indoor RF ability. PLC/RF system configuration does not require the optical detector as in PLC/VLC configuration which is an important feature for the PLC/RF configuration. Motivated by this, researchers have investigated dual-hop RF/PLC systems in a few works [4], [5], [13], [17]. The authors in [5] proposed an efficient and secure solution to guard against availability and privacy attacks for the hybrid RF/PLC system. In [17], the expected data rate of hybrid RF/PLC with and without a relay was investigated, which shows a better performance compared to the non-hybrid system.

In [13], the authors studied the dual-hop hybrid RF/PLC system performance in terms of outage probability, average bit error rate, and average channel capacity, where the log-normal and Nakagami- m distributions characterized the PLC and the RF channels, respectively. In [4], the authors derived the same performance metrics of the dual-hop hybrid RF/PLC system with Log-normal distribution for the PLC link and generalized

Manuscript received September 29, 2021; revised December 3, 2021 and January 20, 2022; accepted March 6, 2022. Date of publication April 5, 2022; date of current version June 24, 2022. The review of this article was coordinated by Dr. Boya Di. (Corresponding author: Basem M. ElHalawany.)

Ahmed Samir, Mohamed Elsayed, and Ahmad A. Aziz El-Banna are with the Benha University, Banha 13511, Egypt (e-mail: ahmed.saied@feng.bu.edu.eg; mohamed.elsayed@feng.bu.edu.eg; ahmad.elbanna@feng.bu.edu.eg).

Kaishun Wu and Basem M. ElHalawany are with the School of Computer Science, Shenzhen University, Shenzhen 518060, China, and also with Benha University, Banha 13511, Egypt (e-mail: basem.mamdoh@feng.bu.edu.eg).

Digital Object Identifier 10.1109/TVT.2022.3165134

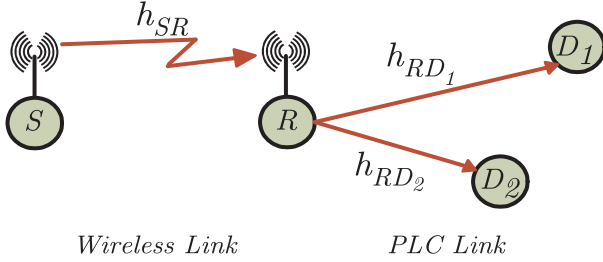


Fig. 1. NOMA based dual-hop hybrid communication system model.

Rician distribution for the RF link. Furthermore, both [4], [13] proposed a system that handles a single destination with no multiplexing capabilities.

In this paper, for the sake of enhancing spectrum efficiency, non-orthogonal multiple access (NOMA) has been proposed to enhance spectrum utilization. The idea behind NOMA is to enable users to communicate with non-orthogonal resources at the expense of higher complexity at the receiver. The most common type of NOMA is the power domain NOMA (PD-NOMA) [18], [19], [26], [27], where the transmission is achieved by superimposing different users' signals at different power levels, while the receivers perform a successive interference cancellation (SIC) to detect their messages. Thus, we investigate NOMA-based dual-hop hybrid RF/PLC communication systems with *DF* relay. While several researchers in the literature have investigated the performance of the hybrid RF-PLC system without utilizing any multiplexing technique [4], [13], to the best of the author's knowledge, there is a gap related to the exploitation of NOMA as an access technique with hybrid RF/PLC.

The main contributions of this paper can be summarized as follows: (1) Derive new closed-form and asymptotic expressions for the outage probability and ergodic capacity under the assumptions that the wireless channel is characterized by Nakagami-*m* fading with an additive white Gaussian noise (AWGN), while the PLC channels are characterized by Log-normal distribution with Bernoulli Gaussian noise including both background and impulsive noise components. (2) Analyze the diversity order of outage probabilities, (3) Propose and solve a power allocation optimization problem for finding an outage-optimal power allocation factor, (4) Confirm our analytical derivations through extensive Monte-Carlo simulations, and finally (5) We study the impact of system parameters on the performance, also a comparison between the proposed system with an OMA-based benchmark system has been carried out.

The rest of the paper is organized as follows. The system model is introduced in Section II. The analytical outage probabilities and ergodic capacities are derived in Section III and IV, respectively. The proposed power allocation algorithm is provided in Section V. Analytical and simulation results are discussed in Section VI and our conclusions are provided in Section VII.

II. SYSTEM MODEL

In this work, we consider a NOMA-based dual-hop hybrid communication system depicted in Fig. 1. A source (*S*) equipped

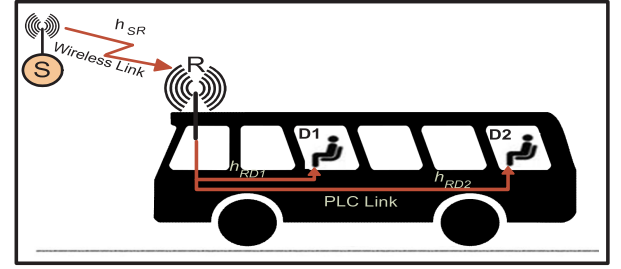


Fig. 2. Illustrative scenario of the vehicle penetration loss in a bus with relay.

with RF interface wants to establish a communication with two destinations (*D*₁ and *D*₂) equipped with PLC interfaces with the help of a *DF* relay node (*R*) that has the ability to interface with both wireless and PLC links. There are several applications of such a scenario, including the communication between a base station and indoor nodes that suffer from high attenuation due to wall penetration loss or in-vehicle communications [20] as the scenario illustrated in Fig. 2. The vehicle is equipped with a *DF* relay node that has an outdoor antenna to interface wirelessly with the source node and has the ability to communicate with in-vehicle users via PLC links equipped in the bus. To improve the spectrum efficiency, *S* transmits a multiplexed signal ($x_S = \sqrt{a_1 P_S} x_1 + \sqrt{a_2 P_S} x_2$) using PD-NOMA through a wireless link, (h_{SR}), to *R* assuming the direct links between *S* and both *D*₁ and *D*₂ are unavailable either due to penetration loss or the absence of wireless interfaces. P_S represents the total transmit power of *S*, while x_j denotes the data symbols of *D*_{*j*} for $j \in \{1, 2\}$, and a_j denotes the power allocation factor of *D*_{*j*}. Without loss of generality, it can be assumed that $a_1 > a_2$ such that $a_1 + a_2 = 1$. The relay node received the following signal through the wireless interface, $y_R = d_w^{-v/2} h_{SR} x_S + n_w$, where d_w is the distance from *S* to *R*, v is wireless channel path-loss exponent, h_{SR} represents the fading of Nakagami-*m* wireless channel with severity factor m_w , such that the expectation $E[|h_{SR}|^2] = \Omega_{SR}$ and n_w denotes AWGN with zero mean, and a variance of σ_w^2 . Therefore, the received signal-to-interference-plus-noise ratio (SINR) at *R* to detect its own message x_1 is given as follows:

$$\gamma_{R,x1} = \frac{a_1 \rho_s d_w^{-v} |h_{SR}|^2}{a_2 \rho_s d_w^{-v} |h_{SR}|^2 + 1}, \quad (1)$$

where $\rho_s = \frac{P_S}{\sigma_w^2}$ is the transmit signal-to-noise ratio (SNR). Then, assuming a perfect SIC, *R* detects x_2 , where the SINR is given as follows

$$\gamma_{R,x2} = a_2 \rho_s d_w^{-v} |h_{SR}|^2. \quad (2)$$

After decoding both messages, *R* re-encodes and multiplexes them using PD-NOMA, where the transmitted message from *R* to both destinations over the PLC interface is given by $x_R = \sqrt{a_1 P_R} x_1 + \sqrt{a_2 P_R} x_2$, and P_R represents the total transmitted power of *R*. Then the received signal at *D*_{*j*} is given by $y_{D_j} = e^{-\theta d_{Pj}} h_{RD_j} x_R + n_p$, where $\theta = \alpha_0 + \alpha_1 f^u$ represents the attenuation over each PLC link, α_0 and α_1 are measurement-based constants, f is the operating frequency, u is the attenuation

factor exponent [22], and d_{Pj} is the distance between R and D_j , h_{RD_j} denotes the Log-normal PLC links, and n_p is a Bernoulli Gaussian noise with a probability distribution function (PDF) [23], [24],

$$f_{(n_p)} = (1-p)CN(0, \sigma_B^2) + pCN(0, \sigma_B^2 + \sigma_I^2), \quad (3)$$

where $CN(0, \sigma)$ stands for the complex Gaussian distribution having zero mean and σ^2 as variance, and p is the probability of the impulsive component of the Bernoulli Gaussian noise. The noise power on the PLC link is σ_B^2 in the presence of only background noise; while the noise power is $\sigma_B^2 + \sigma_I^2 = \sigma_B^2(1+K)$ in the presence of both background and impulsive noises, where $K = \sigma_I^2/\sigma_B^2$ is the impulsive noise index. Then we can write,

$$\sigma_{p_i}^2 = \begin{cases} \sigma_B^2 & \text{Background only, } i = 1 \\ \sigma_B^2(1+K) & \text{Background + impulsive, } i = 2. \end{cases}$$

The SINRs at D_j to detect the message x_1 are given by,

$$\gamma_{i(D_j, x_1)} = \frac{a_1 \rho_{Ri} e^{-2\theta d_{Pj}} |h_{RD_j}|^2}{a_2 \rho_{Ri} e^{-2\theta d_{Pj}} |h_{RD_j}|^2 + 1}, \quad (4)$$

where $\rho_{Ri} = \frac{P_R}{\sigma_{p_i}^2}$ is the transmit SNR at R under a given noise power $\sigma_{p_i}^2$, while D_2 performs SIC to detect its message using the following SINR,

$$\gamma_{i(D_2, x_2)} = a_2 \rho_{Ri} e^{-2\theta d_{P2}} |h_{RD_2}|^2. \quad (5)$$

Channels Distributions: In the following, we highlight the PDFs and the cumulative distribution functions (CDFs) of the channels' gains. Since the wireless channel is characterized by Nakagami- m distribution, $|h_{SR}|^2$ will have a Gamma distribution whose PDF and CDF are [13], [25]:

$$f_{|h_{SR}|^2}(x) = \left(\frac{m_\omega}{\Omega_{SR}}\right)^{m_\omega} \frac{x^{m_\omega-1}}{\Gamma(m_\omega)} e^{-\frac{m_\omega}{\Omega_{SR}}x}, \quad (6)$$

$$F_{|h_{SR}|^2}(x) = 1 - e^{-\left(\frac{m_\omega}{\Omega_{SR}}\right)x} \sum_{m=0}^{m_\omega-1} \frac{\left(\left(\frac{m_\omega}{\Omega_{SR}}\right)x\right)^m}{m!}, \quad (7)$$

On the other hand, the PLC links are characterized by Log-normal distribution with $\mu_{h_{RD_i}}$ mean, and $\sigma_{h_{RD_i}}^2$ variance, so $|h_{RD_i}|^2$ will have a squared Log-normal distribution with the following PDFs [13],

$$f_{|h_{RD_1}|^2}(x) = \frac{1}{\sqrt{2\pi}\sigma'x} e^{-\frac{(\ln(x)-\mu')^2}{2\sigma'^2}}, \quad (8)$$

$$f_{|h_{RD_2}|^2}(x) = \frac{1}{\sqrt{2\pi}\sigma''x} e^{-\frac{(\ln(x)-\mu'')^2}{2\sigma''^2}}, \quad (9)$$

where $\mu' = 2\mu_{h_{RD_1}}$, $\mu'' = 2\mu_{h_{RD_2}}$, $\sigma'^2 = 4\sigma_{h_{RD_1}}^2$, and $\sigma''^2 = 4\sigma_{h_{RD_2}}^2$, while the CDFs are given as follows

$$F_{|h_{RD_1}|^2}(x) = Q\left(\frac{\mu' - \ln(x)}{\sigma'}\right), \quad (10)$$

$$F_{|h_{RD_2}|^2}(x) = Q\left(\frac{\mu'' - \ln(x)}{\sigma''}\right), \quad (11)$$

where $Q(x) = \frac{1}{\sqrt{2\pi}} \int_x^\infty e^{-\frac{t^2}{2}} dt$, is the Gaussian Q -function [29].

III. OUTAGE PROBABILITY ANALYSIS

In this section, we investigate the system performance in terms of the outage probability (OP), which can be defined as the probability that the SINR falls below certain threshold value. In this section, the exact closed form expression for calculating OP of the NOMA based dual-hop hybrid communication system will be derived.

A. Outage Probability at D_1

The OP at D_1 can be expressed in terms of the probability of the impulsive component of the Bernoulli noise (p) as follows:

$$OP_{D_1} = (1-p)OP_{D_1,1} + pOP_{D_1,2}, \quad (12)$$

where $OP_{D_1,i}$ is the OP at D_1 for $\sigma_{p_i}^2$ and $i \in \{1, 2\}$.

The outage event occurs when either D_1 or R can not decode x_1 which can be formulated as follows [30]:

$$\begin{aligned} OP_{D_1,i} &= 1 - \Pr(\gamma_{R,x_1} > \gamma_{th1}, \gamma_{i(D_1,x_1)} > \gamma_{th1}), \\ &\stackrel{(a)}{=} 1 - \Pr\left(|h_{SR}|^2 > \frac{\gamma_{th1}}{\rho_s d_w^v (a_1 - a_2 \gamma_{th1})}\right) \\ &\quad \times \Pr\left(|h_{RD_1}|^2 > \frac{\gamma_{th1}}{\rho_{Ri} e^{-2\theta d_{P1}} (a_1 - a_2 \gamma_{th1})}\right), \end{aligned} \quad (13)$$

where (a) stems from the independence between h_{SR} , h_{RD_1} and substituting (1) and (4) into (13), γ_{th1} is the SINR threshold at D_1 receiver based on a target data rate R_{th1} and $\gamma_{th1} = 2^{2R_{th1}} - 1$. The OP in (13) can be expressed as follows

$$\begin{aligned} OP_{D_1,i} &= 1 - \left(1 - F_{|h_{SR}|^2}\left(\frac{\tau_1}{\rho_s d_w^v}\right)\right) \\ &\quad \times \left(1 - F_{|h_{RD_1}|^2}\left(\frac{\tau_1}{\rho_{Ri} e^{-2\theta d_{P1}}}\right)\right). \end{aligned} \quad (14)$$

such that $a_1 > a_2 \gamma_{th1}$ and $\tau_1 = \frac{\gamma_{th1}}{a_1 - a_2 \gamma_{th1}}$. With the aid of (7) and (10), we can obtain the closed form expression for $OP_{D_1,i}$ as in (15), shown at the bottom of this page.

$$OP_{D_1,i} = 1 - \underbrace{\left(e^{-\left(\frac{m_\omega}{\Omega_{SR}}\right)\left(\frac{\tau_1}{\rho_s d_w^v}\right)}\right)^{m_\omega-1} \sum_{m=0}^{m_\omega-1} \frac{\left(\left(\frac{m_\omega}{\Omega_{SR}}\right)\left(\frac{\tau_1}{\rho_s d_w^v}\right)\right)^m}{m!}}_{\psi_1} \underbrace{Q\left(\frac{\ln\left(\frac{\tau_1}{\rho_{Ri} e^{-2\theta d_{P1}}}\right) - \mu'}{\sigma'}\right)}_{\psi_2} \quad (15)$$

B. Outage Probability at D_2

Similar to (12), the OP at D_2 can be expressed as

$$OP_{D_2} = (1-p)OP_{D_2,1} + pOP_{D_2,2} \quad (16)$$

where $OP_{D_2,1}$ is the OP at D_2 for $\sigma_{p_i}^2$ and $i \in \{1, 2\}$. The outage event occurs when either R or D_2 can not decode x_2 which can be formulated as [30]:

$$\begin{aligned} OP_{D_2,i} &= 1 - \Pr(\gamma_{R,x_1} > \gamma_{th1}, \gamma_{R,x_2} > \gamma_{th2} \\ &\quad \gamma_{i(D_2,x_1)} > \gamma_{th1}, \gamma_{i(D_2,x_2)} > \gamma_{th2}) \end{aligned} \quad (17)$$

where $\gamma_{th2} = 2^{2R_{th2}} - 1$ is the SINR threshold at D_2 for a given target data rate R_{th2} . By substituting (1), (2), (4), and (5) into (17) and exploiting the independence between h_{SR} and h_{RD_2} we get,

$$\begin{aligned} OP_{D_2,i} &= 1 - pr \left(|h_{SR}|^2 > \frac{\delta}{\rho_s d_w^{-v}} \right) \\ &\quad \times pr \left(|h_{RD_2}|^2 > \frac{\delta}{\rho_{Ri} e^{-2\theta d_{P2}}} \right) \\ &= 1 - \left(1 - F_{|h_{SR}|^2} \left(\frac{\delta}{\rho_s d_w^{-v}} \right) \right) \\ &\quad \times \left(1 - F_{|h_{RD_2}|^2} \left(\frac{\delta}{\rho_{Ri} e^{-2\theta d_{P2}}} \right) \right) \end{aligned} \quad (18)$$

where $a_1 > a_2 \gamma_{th1}$, $\tau_1 = \frac{\gamma_{th1}}{a_1 - a_2 \gamma_{th1}}$ and $\tau_2 = \frac{\gamma_{th2}}{a_2}$, and $\delta = \max(\tau_1, \tau_2)$. With the aid of (7) and (11), we can obtain the closed form expression for $OP_{D_2,i}$ as in (19) shown at the bottom of this page.

C. Total System Outage Probability

Similarly, The total system OP can be expressed as,

$$OP_{sys} = (1-p)OP_{sys,1} + pOP_{sys,2} \quad (20)$$

where $OP_{sys,i}$ is the system OP for $\sigma_{p_i}^2$ and $i \in \{1, 2\}$, which occurs when any of R or D_2 can not detect the two messages or

D_1 can not detect x_1 . $OP_{sys,i}$ can be expressed as,

$$\begin{aligned} OP_{sys,i} &= 1 - \Pr(\gamma_{R,x_1} > \gamma_{th1}, \gamma_{R,x_2} > \gamma_{th2}, \\ &\quad \gamma_{i(D_2,x_1)} > \gamma_{th1}, \gamma_{i(D_2,x_2)} > \gamma_{th2}, \\ &\quad \gamma_{i(D_1,x_1)} > \gamma_{th1}). \\ &\stackrel{(b)}{=} 1 - OP_{D_2,i} \times \Pr(|h_{RD_1}|^2 > \frac{\tau_1}{\rho_{Ri} e^{-2\theta d_{P1}}}). \end{aligned} \quad (21)$$

where (b) stems from the independence of h_{SR} , h_{RD_1} , and h_{RD_2} . Finally the closed-form expression for $OP_{sys,i}$ can be expressed as in (22) shown at the bottom of this page.

D. Asymptotic Outage Probability

In order to gain insights and understand the effects of different parameters on the performance of our system, we derive the asymptotic OPs for high values of the transmit SNRs. As $\rho_s \rightarrow \infty$, based on [31, eq. 20] we can write ψ_1^∞ and θ_1^∞ as follows,

$$\psi_1^\infty = 1 - \frac{1}{m_\omega!} \left((m_\omega / \Omega_{SR}) \frac{\tau_1}{\rho_s d_m^{-v}} \right)^{m_\omega} \quad (23)$$

$$\theta_1^\infty = 1 - \frac{1}{m_\omega!} \left((m_\omega / \Omega_{SR}) \frac{\delta}{\rho_s d_m^{-v}} \right)^{m_\omega}. \quad (24)$$

As $\rho_{Ri} \rightarrow \infty$, based on [32, eq. 43] $Q(x) = \frac{e^{-\frac{x^2}{2}}}{x\sqrt{2\pi}}$ when $x \rightarrow \infty$ we can write ψ_2^∞ and θ_2^∞ as follows,

$$\psi_2^\infty = 1 - \frac{\sigma' e^{-\frac{\left(\mu' + \ell n \left(\frac{\rho_{Ri} e^{-2\theta d_{P1}}}{\tau_1} \right)\right)^2}{2\sigma'^2}}}{\sqrt{2\pi} \left(\mu' + \ell n \left(\frac{\rho_{Ri} e^{-2\theta d_{P1}}}{\tau_1} \right) \right)}, \quad (25)$$

$$\theta_2^\infty = 1 - \frac{\sigma'' e^{-\frac{\left(\mu'' + \ell n \left(\frac{\rho_{Ri} e^{-2\theta d_{P2}}}{\delta} \right)\right)^2}{2\sigma''^2}}}{\sqrt{2\pi} \left(\mu'' + \ell n \left(\frac{\rho_{Ri} e^{-2\theta d_{P2}}}{\delta} \right) \right)}. \quad (26)$$

$$OP_{D_2,i} = 1 - \underbrace{\left(e^{\left(\frac{-m_\omega}{\Omega_{SR}} \left(\frac{\delta}{\rho_s d_w^{-v}} \right) \right)} \sum_{m=0}^{m_\omega-1} \frac{\left((m_\omega / \Omega_{SR}) \left(\frac{\delta}{\rho_s d_w^{-v}} \right) \right)^m}{m!} \right)}_{\theta_1} \underbrace{Q \left(\frac{\ell n \left(\frac{\delta}{\rho_{Ri} e^{-2\theta d_{P2}}} \right) - \mu''}{\sigma''} \right)}_{\theta_2} \quad (19)$$

$$OP_{sys,i} = 1 - \underbrace{\left(e^{\left(\frac{-m_\omega}{\Omega_{SR}} \left(\frac{\delta}{\rho_s d_w^{-v}} \right) \right)} \sum_{m=0}^{m_\omega-1} \frac{\left((m_\omega / \Omega_{SR}) \left(\frac{\delta}{\rho_s d_w^{-v}} \right) \right)^m}{m!} \right)}_{\theta_1} \underbrace{Q \left(\frac{\ell n \left(\frac{\delta}{\rho_{Ri} e^{-2\theta d_{P2}}} \right) - \mu''}{\sigma''} \right)}_{\theta_2} \underbrace{Q \left(\frac{\ell n \left(\frac{\tau_1}{\rho_{Ri} e^{-2\theta d_{P1}}} \right) - \mu'}{\sigma'} \right)}_{\psi_2} \quad (22)$$

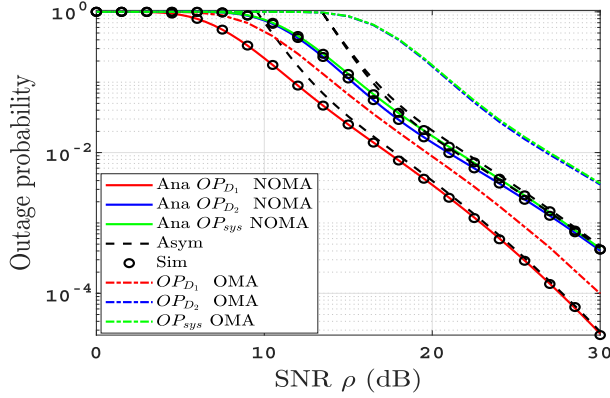


Fig. 3. OP versus SNR (ρ) with $K = 3$, $R_{th1} = 0.5$, $R_{th2} = 0.75$, and $p = 0.1$.

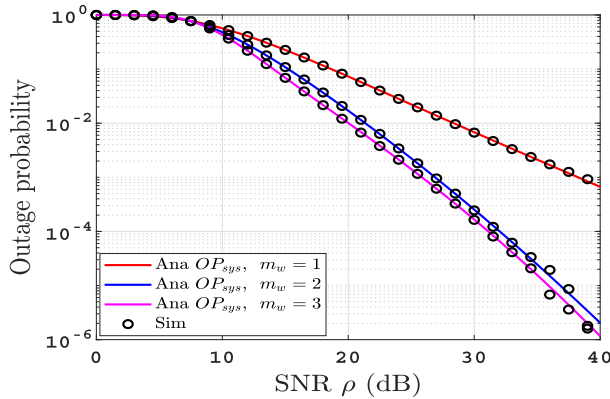


Fig. 4. OP with different value of m_w at $p = 0.1$, $K = 10$, and $a_1 = 0.72$.

Thus, the asymptotic OPs can be expressed as follows:

$$\begin{aligned} OP_{D1,i}^\infty &\approx 1 - \psi_1^\infty \psi_2^\infty \\ OP_{D2,i}^\infty &\approx 1 - \theta_1^\infty \theta_2^\infty \\ OP_{sys,i}^\infty &\approx 1 - \theta_1^\infty \theta_2^\infty \psi_2^\infty \end{aligned} \quad (27)$$

Finally we can write

$$\begin{aligned} OP_{D1}^\infty &= (1-p)OP_{D1,1}^\infty + pOP_{D1,2}^\infty \\ OP_{D2}^\infty &= (1-p)OP_{D2,1}^\infty + pOP_{D2,2}^\infty \\ OP_{sys}^\infty &= (1-p)OP_{sys,1}^\infty + pOP_{sys,2}^\infty \end{aligned} \quad (28)$$

E. Diversity Order

To obtain further insights, we consider the achievable diversity order of the proposed system outage probability which is defined as the slope of its OP_{sys} , and based on [20], [30], we can calculate diversity order as $d_{OP} = -\lim_{\rho \rightarrow \infty} (\log(OP_l^\infty)/\log(\rho))$ where $l \in \{1, 2, sys\}$. It is clear from (15), (19), (22), and (27) that $d_{OP} \propto \rho^{-\min(m_w, 2)}$, which means $d_{OP} = \min(m_w, 2)$. This result is consistent with the plots in Fig. 4.

IV. ERGODIC CAPACITY

In this section, we derive a closed-form expression of the ergodic capacity (EC) of the considered NOMA-based dual-hop hybrid RF-PLC communication system. The channel capacities

for both messages, C_{x_1} and C_{x_2} are determined by the weaker link [33], [34], thus

$$\begin{aligned} C_{x_1} &= \frac{1}{2} \log_2(1 + \min(\gamma_{R,x_1}, \gamma_{D1,x_1}, \gamma_{D2,x_1})) \\ C_{x_2} &= \frac{1}{2} \log_2(1 + \min(\gamma_{R,x_2}, \gamma_{D2,x_2})). \end{aligned} \quad (29)$$

The EC , which is the expectation of the channel capacity, can be expressed based on the impulsive component arrival probability of the Bernoulli noise (p) as follows [13], [34]

$$EC_{x_j} = (1-p)EC_{x_j,1} + (p)EC_{x_j,2} \quad (30)$$

$$EC_{x_j,i} = \frac{1}{2\ln 2} \int_{\gamma=0}^{\infty} \frac{1}{1+\gamma} [1 - F_{\gamma_j,i}(\gamma)] d\gamma. \quad (31)$$

The ergodic sum capacity (ESC) is expressed as

$$ESC = EC_{x_1} + EC_{x_2}. \quad (32)$$

A. Ergodic Capacity of x_1

The CDF $F_{\gamma_1,i}(\gamma)$ can be written as

$$\begin{aligned} F_{\gamma_1,i}(\gamma) &= 1 - \text{pr}(\gamma_{R,x_1} > \gamma, \gamma_{D1,x_1} > \gamma, \gamma_{D2,x_1} > \gamma) \\ &\stackrel{(c)}{=} 1 - \text{pr}(|h_{SR}|^2 > \frac{\eta}{\rho_s d_w^{-v}}) \text{pr}(|h_{RD1}|^2 > \\ &\quad \frac{\eta}{\rho_{Ri} e^{-2\theta d_{P1}}} \text{pr}(|h_{RD2}|^2 > \frac{\eta}{\rho_{Ri} e^{-2\theta d_{P2}}}), \end{aligned} \quad (33)$$

where (c) stems from the independence of the channels gain and $\eta = \gamma/(a_1 - a_2\gamma)$, and $\eta > 0$ or $0 < \gamma < \frac{a_1}{a_2}$, then using (7), (10) and (11) we get

$$\begin{aligned} F_{\gamma_1,i}(\gamma) &= 1 - e^{\left(\frac{-m_w \eta}{\Omega_{SR} \rho_s d_w^{-v}}\right)} \sum_{m=0}^{m_w-1} \frac{\left(\frac{m_w \eta}{\rho_s d_w^{-v} \Omega_{SR}}\right)^m}{m!} \\ &\quad \times Q\left(\frac{\ln\left(\frac{\eta}{\rho_{Ri} e^{-2\theta d_{P1}}}\right) - \mu'}{\sigma'}\right) Q\left(\frac{\ln\left(\frac{\eta}{\rho_{Ri} e^{-2\theta d_{P2}}}\right) - \mu''}{\sigma''}\right). \end{aligned} \quad (34)$$

Substituting form (34) in (31) then

$$\begin{aligned} EC_{x_1,i} &= \frac{1}{2\ln 2} \int_{\gamma=0}^{a_1/a_2} \frac{e^{\left(\frac{-m_w \eta}{\Omega_{SR} \rho_s d_w^{-v}}\right)} \sum_{m=0}^{m_w-1} \frac{\left(\frac{m_w \eta}{\rho_s d_w^{-v} \Omega_{SR}}\right)^m}{m!} \times \\ &\quad Q\left(\frac{\ln\left(\frac{\eta}{\rho_{Ri} e^{-2\theta d_{P1}}}\right) - \mu'}{\sigma'}\right) Q\left(\frac{\ln\left(\frac{\eta}{\rho_{Ri} e^{-2\theta d_{P2}}}\right) - \mu''}{\sigma''}\right) d\gamma, \end{aligned} \quad (35)$$

using variable transformation of $t = m_w \eta / (\rho_s d_w^{-v} \Omega_{SR})$ we can write

$$EC_{x_1,i} = \frac{a_1 \rho_s d_w^{-v} m_w \Omega_{SR}}{2\ln 2} \sum_{m=0}^{m_w-1} \frac{1}{m!} \int_{t=0}^{\infty} e^{-t} f_1(t) dt, \quad (36)$$

where

$$f_1(t) = \frac{t^m Q\left(\frac{\ln\left(\frac{\beta t}{e^{-2\theta d P_1}}\right) - \mu'}{\sigma'}\right) Q\left(\frac{\ln\left(\frac{\beta t}{e^{-2\theta d P_2}}\right) - \mu''}{\sigma''}\right)}{(t\rho_s d_w^{-v} \Omega_{SR} + m_\omega)(t\rho_s d_w^{-v} \Omega_{SR} a_2 + m_\omega)}, \quad (37)$$

where $\beta = \frac{\rho_s d_w^{-v} \Omega_{SR}}{\rho_{Ri} m_\omega}$. The integration in (36) can not admit closed-form expression, however, it can be approximated using [[35], eq. (25.4.45)]. We can write

$$EC_{x_1,i} = \frac{a_1 \rho_s d_w^{-v} m_\omega \Omega_{SR}}{2\ell n 2} \sum_{m=0}^{m_\omega-1} \sum_{i=1}^n \frac{w_i f_1(t_i)}{m!} \quad (38)$$

where t_i is the i^{th} zero of the Laguerre polynomial, $L_n(x)$, while w_i is the weights that can be calculated as follows:

$$w_i = \frac{(n!)^2 x_i}{(n+1)^2 [L_{n+1}(x_i)]^2} \quad (39)$$

B. Ergodic Capacity of x_2

The CDF $F_{\gamma_2,i}(\gamma)$ can be written as

$$\begin{aligned} F_{\gamma_2,i}(\gamma) &= 1 - pr(\gamma_{R,x_2} > \gamma, \gamma_{D_2,x_2} > \gamma) \\ &\stackrel{(d)}{=} 1 - pr(|h_{SR}|^2 > \frac{\gamma}{a_2 \rho_s d_w^{-v}}) \\ &\quad \times pr(|h_{RD_2}|^2 > \frac{\gamma}{a_2 \rho_{Ri} e^{-2\theta d P_2}}) \end{aligned} \quad (40)$$

where (d) stems from the independence of the channels gain then using (7) and (11) we get

$$\begin{aligned} F_{\gamma_2,i}(\gamma) &= 1 - e\left(\frac{-m_\omega \gamma}{a_2 \Omega_{SR} \rho_s d_w^{-v}}\right) \sum_{m=0}^{m_\omega-1} \frac{\left(\frac{m_\omega \gamma}{a_2 \Omega_{SR} \rho_s d_w^{-v}}\right)^m}{m!} \\ &\quad \times Q\left(\frac{\ln\left(\frac{\gamma}{a_2 \rho_{Ri} e^{-2\theta d P_2}}\right) - \mu''}{\sigma''}\right). \end{aligned} \quad (41)$$

Substituting form (41) in (31) then

$$\begin{aligned} EC_{x_2,i} &= \frac{1}{2\ell n 2} \int_{\gamma=0}^{\infty} \frac{e\left(\frac{-m_\omega \gamma}{a_2 \Omega_{SR} \rho_s d_w^{-v}}\right)}{1 + \gamma} \sum_{m=0}^{m_\omega-1} \frac{\left(\frac{m_\omega \gamma}{a_2 \Omega_{SR} \rho_s d_w^{-v}}\right)^m}{m!} \\ &\quad \times Q\left(\frac{\ln\left(\frac{\gamma}{a_2 \rho_{Ri} e^{-2\theta d P_2}}\right) - \mu''}{\sigma''}\right) d\gamma, \end{aligned} \quad (42)$$

using variable transformation of $\lambda = m_\omega \gamma / (a_2 \Omega_{SR} \rho_s d_w^{-v})$ we can write

$$EC_{x_2,i} = \frac{a_2 \rho_s d_w^{-v} \Omega_{SR}}{2\ell n 2} \sum_{m=0}^{m_\omega-1} \frac{1}{m!} \int_{t=0}^{\infty} e^{-\lambda} f_2(\lambda) d\lambda, \quad (43)$$

where

$$f_2(\lambda) = \frac{\lambda^m Q\left(\frac{\ln\left(\frac{\beta \lambda}{e^{-2\theta d P_2}}\right) - \mu''}{\sigma''}\right)}{(\lambda \rho_s d_w^{-v} \Omega_{SR} a_2 + m_\omega)}. \quad (44)$$

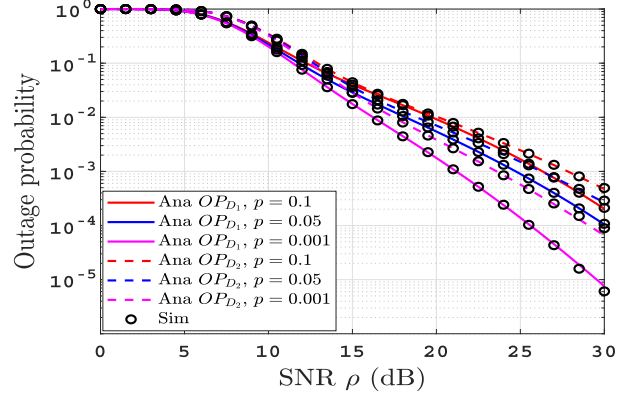


Fig. 5. OP with different value of p with $K = 10$, $\gamma_{th} = 1$, and $a_1 = 0.72$.

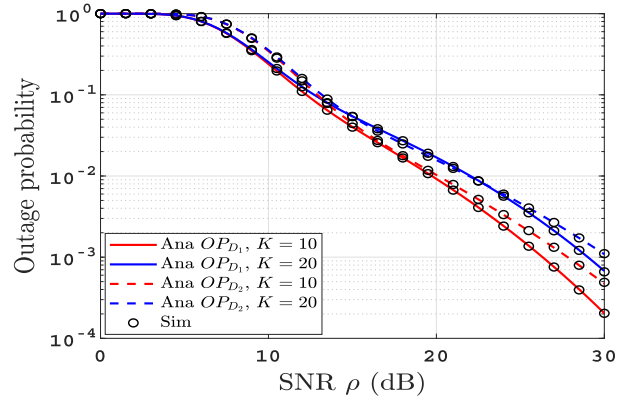


Fig. 6. OP with different values of K at $p = 0.1$, $\gamma_{th} = 1$, and $a_1 = 0.72$.

Using the same procedure of Laguerre formula in IV-A, then

$$EC_{x_2,i} = \frac{a_2 \rho_s d_w^{-v} \Omega_{SR}}{2\ell n 2} \sum_{m=0}^{m_\omega-1} \sum_{i=1}^n \frac{w_i f_2(\lambda_i)}{m!} \quad (45)$$

V. PROPOSED POWER ALLOCATION ALGORITHM

In this section, we discuss a proposed power allocation algorithm for optimizing the outage probability of the system. The proposed optimization problem is given as follows:

$$\min_{a_1} OP_{sys} \quad (46a)$$

$$\text{s.t. } 0.5 < a_1 < 1 \quad (46b)$$

$$a_1 + a_2 = 1 \quad (46c)$$

In the following, we provide Theorem 1 to prove the convexity of the problem.

Theorem 1: The problem in (46) is a convex optimization problem.

Proof: Please, refer to the Appendix. ■

Since (46) is a convex optimization problem, it can be solved using any commercial solver such as Matlab or Mathematica. With the system parameters setting defined in Table I, we show the variations of the system OP as a function of a_1 in Fig. 8, to show the convexity graphically. The solution of such problem

TABLE I
PARAMETER VALUES USED FOR SIMULATIONS

Parameter value used	p	K	m_w	σ' (dB)	σ'' (dB)	μ'	μ''	Ω_{SR}	a_1	γ_{th}	ρ_s (dB)	f (kHz)	α_0	α_1	u	$d_{P1}(m)$	$d_{P2}(m)$	$d_w(m)$	v
	0.1, 0.05, 0.001	3, 10, 20	2, 4	2	3	1	2	2	0.5, 0.99	0.5, 0.75, 1	0, 30	100	$2.03e-3$	$3.75e-7$	0.4	7	10	2	2

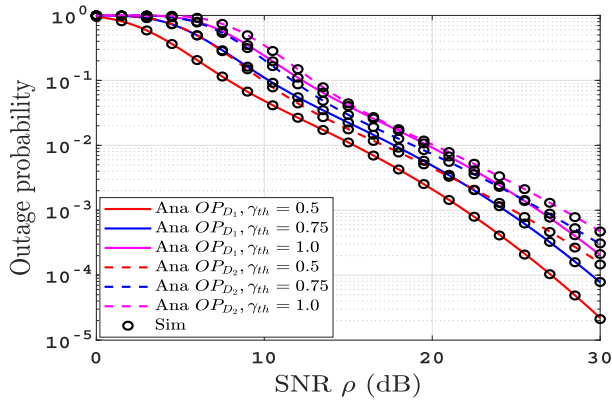


Fig. 7. OP with different values of γ_{th} at $p = 0.1$, $K = 10$, and $a_1 = 0.72$.

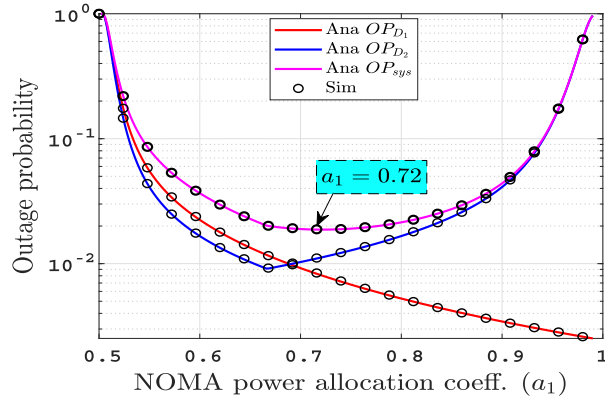


Fig. 8. OP with different value of a_1 at $\rho = 20$ dB, $p = 0.1$, and $K = 10$.

gives an optimal value for power allocation factor as $a_1 = 0.72$. This solution is used as an optimal power allocation scheme in all figures in Section VI.

VI. RESULTS AND DISCUSSIONS

In this section, we provide representative numerical results to illustrate the derived OP_s metrics, based on which some insights are highlighted. Monte Carlo simulations are generated to corroborate the proposed analysis. Unless mentioned otherwise, the simulation parameters used in the plots are given in Table I, which are based on [13], [36], and [37], where $\gamma_{th} = \gamma_{th1} = \gamma_{th2}$. In the following simulation figures, we denote ‘‘Ana’’ as the exact analytical results, ‘‘Asym’’ denotes the asymptotic results, and ‘‘Sim’’ denotes Monte-Carlo simulation results. We have assumed that $\rho_s = \rho_{R1} = \rho$, while $\rho_{R2} = \frac{\rho}{(1+K)}$.

In Fig. 3, the OP_s at D_1 , D_2 and total system outage OP_{sys} versus SNR (ρ) for $K = 3$, $\gamma_{th} = 1$, $a_1 = 0.72$, and $p = 0.1$ are represented. The results show that the simulation results perfectly coincide with the exact analytical results for the whole range of ρ , thereby validating our analysis. Also, we note that the

asymptotic curves are matched with both the exact and simulation curves at high SNR. Additionally, the results show that both OP_s improve as ρ increases. To evaluate the performance of the proposed system in this work, we compared its performance with a benchmark scheme; OMA based dual-hop hybrid communication system. Fig. 3 demonstrates the comparison between the proposed NOMA-based system versus the OMA-based system in terms of outage probability under the same system settings. According to the figure, the proposed system outperformed the benchmark in terms of OP_{D1} , OP_{D2} , and OP_{sys} , the reason that explains this discrepancy is that the NOMA-based system is spectrum-efficiency by exploiting the power domain. From the comparison, we can conclude that the NOMA-based system outperformed the OMA-based benchmark system.

It is seen from Fig. 4 that as the value of m_w increases the OP_{sys} performance of the system enhances due to the fact that the severity of fading decreases with increasing m_w . Also we can notice that for $m_w = 1$ the $OP_{sys} = 0.006937$ at $\rho = 30$ dB while $OP_{sys} = 0.0006676$ at $\rho = 40$ dB, so the OP_{sys} falls with slope of $\log(0.0006676) - \log(0.006937) \approx 1 = m_w$. Following the same procedure for the other two values of m_w , we can observe that both curves have the same slope = 2 at high SNR and agree with the diversity order calculated in Section III-E.

Fig. 5 shows the OP_s of both users under various values of PLC impulsive noise arrival probability (p) for $K = 10$, $\gamma_{th} = 1$, and $a_1 = 0.72$. The results show that as p decreases, the OP improves which draws attention to the effect of the impulsive noise on the PLC channels. The effect of the impulsive noise index (K) on the OP_s of both users is investigated in Fig. 6. By setting $p = 0.1$, $\gamma_{th} = 1$, and $a_1 = 0.72$, and keeping the background noise fixed, it is shown that having a lower value of $K = 10$ leads to a better OP compared to higher values of $K = 20$, which is expected since increasing K raises the total noise.

Fig. 7 shows the effect of the SNR threshold for the OP_s of both users. The results show the OP_s of both users versus ρ for $\gamma_{th} = 0.5, 0.75$, and 1 assuming $p = 0.1$, $K = 10$, and $a_1 = 0.72$. It is shown that the OP_s degrades with the increase of the target threshold.

Fig. 8 plots the influence of power allocation parameter a_1 ; which varies from 0.5 to 0.99; on the OP performance with $\rho = 20$ dB, $p = 0.1$, and $K = 10$. We can see that the OP for D_1 improves with increasing a_1 due to increase of its own message power and the decrease of interference power from D_2 . On the other hand, the OP of D_2 shows an improvement at first with a_1 increase since D_2 needs to decode $x_1(t)$ first before decoding its own message. However, with the continuous increase in a_1 , an inflection point is reached since increasing a_1 means decreasing the allocated power for D_2 message ($a_2 = 1 - a_1$) which deteriorates the OP of D_2 . Additionally, the total system OP follows the same behavior as OP at D_2 with a slight increase

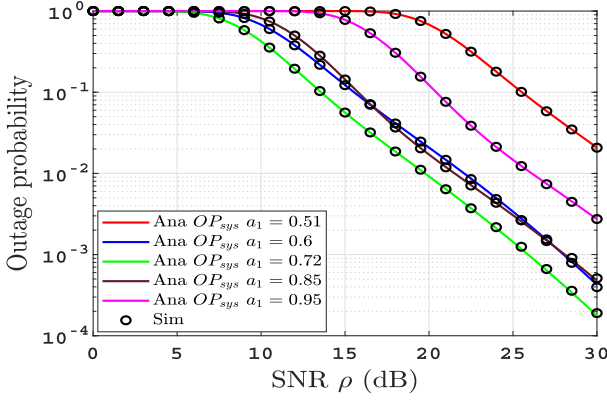


Fig. 9. System outage probability for different values of a_1 against the optimal value for $K = 2$ and $p = 0.05$.

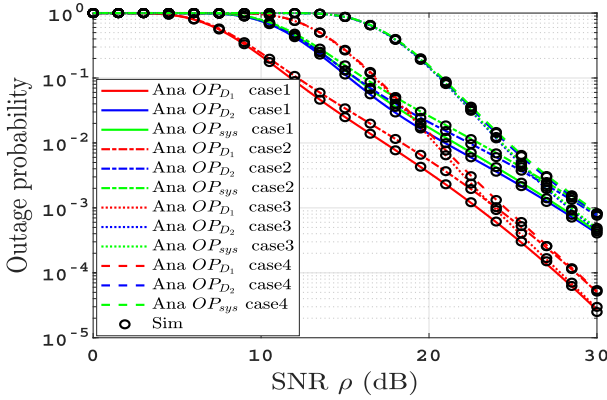


Fig. 10. The effect of changing d_{p1} , d_{p2} , and d_w on OPs at $a_1 = 0.72$, $p = 0.1$, and $K = 3$.

in the OP value. Under the pre-mentioned settings, the system OP shows an optimal value for the power allocation parameter at $a = 0.72$, which suggests that we can tweak the power allocation factor to get an outage-optimal value.

To confirm the results, we plotted Fig. 9 which represents system outage probability for different values of a_1 including inferred optimal value. And we will already notice from Fig. 9 that the inferred optimal value gives the best result for OP_{sys} .

Fig. 10 depicts the effect of changing the distances between the nodes of the system on the OPs . In the figure, we can find four different cases, the first case represents the reference case in which we set $d_{p1} = 7\text{ m}$, $d_{p2} = 10\text{ m}$ and $d_w = 2\text{ m}$. The second case studies the effect of increasing the lengths of PLC links to ten-folds of their reference lengths, it is clear that the effect is negligible at low SNR while OPs degrade slightly at high SNR. The situation in case 3 is inverted when we duplicate the wireless channel length while keeping PLC links at the reference values, where the OPs witnessed a large degradation at low SNR and coincide with the reference curve at high SNR. In the last case, we composite the two modifications carried out in case 2 and case 3 to illustrate the effect of increasing all distances on the OPs , here we can notice the large degradation at low SNR due to the

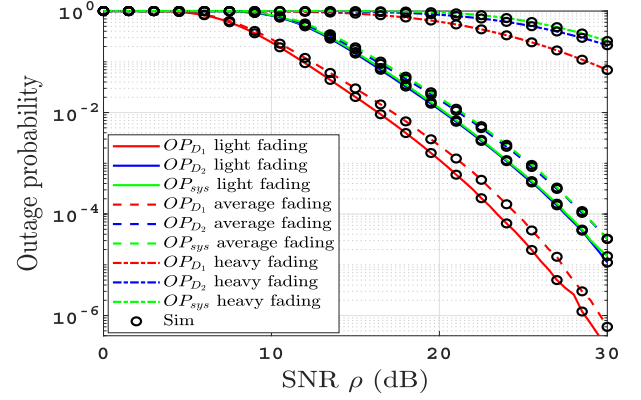


Fig. 11. The effect of changing fading parameters on OPs at $a_1 = 0.72$, $p = 0.1$, and $K = 3$.

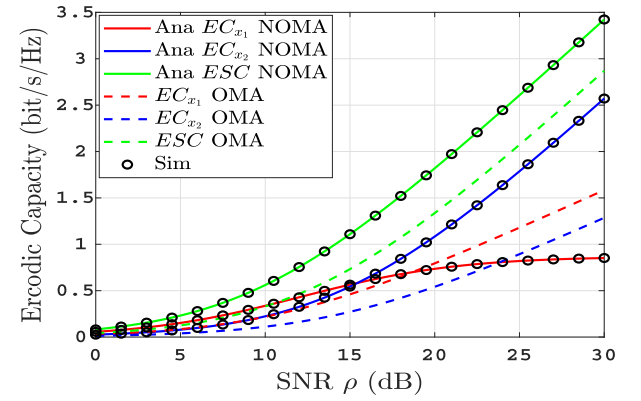


Fig. 12. EC versus SNR (ρ) with $K = 2$, $a_1 = 0.72$, and $p = 0.05$.

increase in wireless channel distance, and the slight degradation at high SNR due to the increase in the lengths of the PLC links.

Fig. 11 depicts the Log-normal fading parameters effect on the OPs performance, using three different scenarios (light shadowing with $\mu' = \mu'' = 0.115$ and $\sigma' = \sigma'' = 0.115\text{ dB}$, average shadowing with $\mu' = \mu'' = -0.115$ and $\sigma' = \sigma'' = 0.161\text{ dB}$, heavy shadowing with $\mu' = \mu'' = -3.914$ and $\sigma' = \sigma'' = 0.806\text{ dB}$ as in literature [38]). It is clear from the figure that, the OPs deteriorates with the increase in the shadowing parameters, which leads to the failure in achieving target threshold SNR as shadowing rises from light to heavy shadowing scenario.

Fig. 12 depicts the EC of both messages and the ESC versus the SNR. We can see that the EC_{x1} increases slightly in the low-SNR region and remain constants in the high-SNR region due to the saturation of $\gamma_{R,x1}$, $\gamma_{i(Dj,x1)}$ in (1), (4) to the value of (a_1/a_2) . On the other hand, EC_{x2} continuously increases with the increase in SNR, this result can be deduced by examining equations (2) and (5). Although the performance of EC for each message is different, the performance of ESC follows the trend of EC_{x2} . Also in the same figure, we compare the performance of EC and ESC for both systems under the same values of system parameters. Although the performance of the two systems contrasted from the point of view of the ergodic capacity for each message; as the proposed system based on

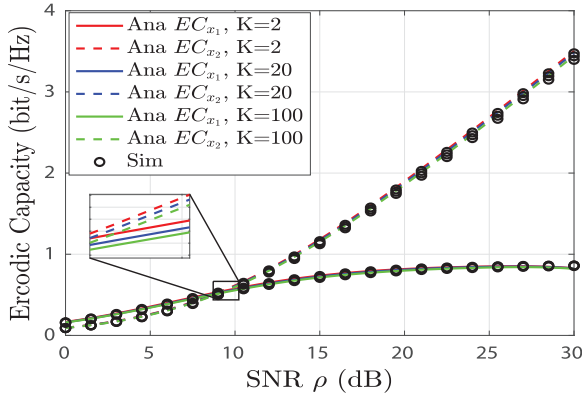


Fig. 13. EC with different values of K at $p = 0.05$ and $a_1 = 0.72$.

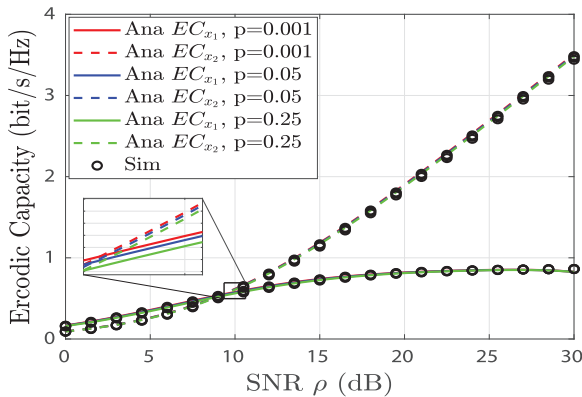


Fig. 14. EC with different value of p with $K = 2$ and $a_1 = 0.72$.

NOMA outperformed its counterpart based on OMA for the EC_{x_2} , in contrast to the situation for the EC_{x_1} ; in general the NOMA-based system superior the OMA-based in terms of ergodic sum capacity. This logical conclusion came as a result of the idea that NOMA allows multiple users to share the given channel resources concurrently unlike OMA. From the comparison carried out between the two systems in Fig. 3 and Fig. 12, we can conclude that the NOMA-based system outperformed the OMA-based benchmark system.

To study the effect of some system parameters variation, we plot Fig. 13 and Fig. 14. Fig. 13 demonstrates the effect of the impulsive noise index on the EC as a function of SNR for $p = 0.05$ and $a_1 = 0.72$. We notice that the EC of the system slightly increases with a huge decrease in K from 100 to 2. Also, Fig. 14 shows the influence of impulsive noise arrival probability on the EC as a function of SNR for $K = 2$ and $a_1 = 0.72$. We observe the similarity between the impacts of K and p on EC . As expected, the EC is higher for lower values of p compared to higher values. From both figures, we can conclude that the effect of both the impulsive noise index and the impulsive noise arrival probability is negligible.

Fig. 15 shows the effect of changing the distances between the nodes of the system on the EC s. In this figure, four different cases are represented, the first case is the reference case in which we set $d_{p_1} = 7 m$, $d_{p_2} = 10 m$ and $d_w = 2 m$. The second case studies the effect of increasing the lengths of PLC links to $d_{p_1} =$

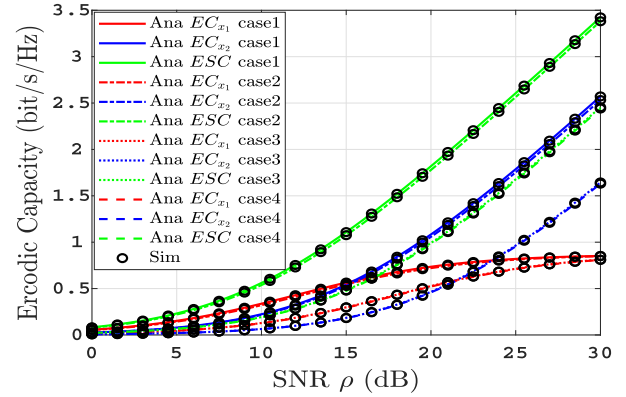


Fig. 15. The effect of changing d_{p_1} , d_{p_2} , and d_w on EC s at $a_1 = 0.72$, $p = 0.1$, and $K = 2$.

$200 m$, $d_{p_2} = 300 m$ and $d_w = 2 m$, it is clear that the effect is negligible over the entire range of SNR. The situation in case 3; when we duplicate the wireless channel length while keeping PLC links at the reference values; is that the EC s witnessed a large degradation due to the increase in channel fading. In the last case, we composite the two modifications carried out in case 2 and case 3 to illustrate the effect of increasing all distances on the EC s, so we used $d_{p_1} = 200 m$, $d_{p_2} = 300 m$ and $d_w = 4 m$, here we can notice the small deviation between the last two cases which confirms the aforementioned result in case 2, that the effect of increasing the length of the PLC links can be neglected.

VII. CONCLUSION

In this paper, we investigated a novel two-users NOMA-based dual-hop hybrid RF-PLC communication system utilizing a DF relay. We derived new analytical closed-form expressions for the OP s, the asymptotic OP s of the two users, and ergodic capacities, also analyzed the diversity order for the OP s. Additionally, we confirm our expressions through representative Monte-Carlo simulations. It is inferred from figures that as the arrival probability of the impulsive noise or the impulsive noise index increases, the OP s of the two users and the system degrade, on the other hand, the ergodic capacities witnessed no noticeable change. Besides, we discussed the influence of the power allocation factor on the total system OP performance and obtaining an outage-optimal power allocation. Finally, we carried out a comparison between the proposed system and a benchmark system, and it proved the importance and superiority of the proposed system.

APPENDIX A

In this appendix, a detailed derivation that prove the convexity of the problem described in (46). Based on (20), we can write $OP'_{sys} = (1 - p)OP'_{sys,1} + (p)OP'_{sys,2}$, thus we need to prove convexity of $OP'_{sys,i}$.

According to the definition of $\delta = \max(\tau_1, \tau_2)$, we can divide (22) into two intervals based on the value of a_1 :

• For $0.5 < a_1 < \frac{\gamma_{th1}(1+\gamma_{th2})}{\gamma_{th1}+\gamma_{th2}+\gamma_{th1}\gamma_{th2}}$: In this interval $\tau_1 > \tau_2$ and $\delta = \tau_1 = \frac{\gamma_{th1}}{a_1(1+\gamma_{th1})-\gamma_{th1}}$, and using ([32], eq. (43)), where $Q(x) = (e^{-x^2/2}/x\sqrt{2\pi})$, we can rewrite (22) as

$$OP_{sys,i} = 1 - \underbrace{e^{-c_1\tau_1}}_{\phi_1} \sum_{m=0}^{m_w-1} \underbrace{\frac{(c_1\tau_1)^m}{m!}}_{\phi_2} \underbrace{\frac{e^{-x_{1,i}^2/2}}{x_{1,i}\sqrt{2\pi}}}_{\phi_3} \underbrace{\frac{e^{-x_{2,i}^2/2}}{x_{2,i}\sqrt{2\pi}}}_{\phi_4}, \quad (\text{A.1})$$

where $c_1 = \frac{m_w}{\Omega_{SR}\rho_s d_w^{-\nu}}$, $x_{1,i} = \frac{\ln(\frac{\tau_1}{\rho_{Ri}e^{-2\theta d_{P1}}}) - \mu'}{\sigma'}$, $x_{2,i} = \frac{\ln(\frac{\tau_1}{\rho_{Ri}e^{-2\theta d_{P2}}}) - \mu''}{\sigma''}$. Using $Q'(x) = \frac{-e^{-x^2/2}}{\sqrt{2\pi}}$, we can write the partial derivative of $OP_{sys,i}$ with respect to τ_1 as

$$\begin{aligned} \frac{\partial OP_{sys,i}}{\partial \tau_1} &= \\ &-(-c_1\phi_1\phi_2\phi_3\phi_4 + \phi_1 \left[c_1(\phi_2 - \frac{(c_1\tau_1)^{m_w-1}}{(m_w-1)!}) \right] \phi_3\phi_4 \\ &+ \phi_1\phi_2 \left[\frac{-e^{-x_{1,i}^2/2}}{\tau_1\sigma'\sqrt{2\pi}} \right] \phi_4 + \phi_1\phi_2\phi_3 \left[\frac{-e^{-x_{2,i}^2/2}}{\tau_1\sigma''\sqrt{2\pi}} \right]) \\ &= \phi_1\phi_3\phi_4 \left(\frac{c_1^{m_w}\tau_1^{m_w-1}}{(m_w-1)!} + \frac{\phi_2}{\tau_1\sigma'}(x_{1,i} + x_{2,i}) \right) > 0, \quad (\text{A.2}) \end{aligned}$$

it is clear that $\frac{\partial OP_{sys,i}}{\partial \tau_1}$ in (A.2) is always a positive value. Applying the chain rule, $\frac{\partial OP_{sys,i}}{\partial a_1} = \frac{\partial OP_{sys,i}}{\partial \tau_1} \times \frac{\partial \tau_1}{\partial a_1}$, where $\frac{\partial \tau_1}{\partial a_1} = \frac{-(1+\gamma_{th1})\gamma_{th1}}{(a_1(1+\gamma_{th1})-\gamma_{th1})^2}$ is a negative value. Thus, $\frac{\partial OP_{sys,i}}{\partial a_1}$ is always negative, this result indicates a monotonically decreasing function in this interval.

• For $\frac{\gamma_{th1}(1+\gamma_{th2})}{\gamma_{th1}+\gamma_{th2}+\gamma_{th1}\gamma_{th2}} < a_1 < 1$: In this interval $\tau_1 < \tau_2$ and $\delta = \tau_2 = \frac{\gamma_{th2}}{1-a_1}$, then we can rewrite (22) as

$$OP_{sys,i} = 1 - \underbrace{e^{-\frac{c_2}{1-a_1}}}_{\phi_5} \sum_{m=0}^{m_w-1} \underbrace{\frac{c_2^m}{m!(1-a_1)^m}}_{\phi_6} \underbrace{\frac{e^{-x_{3,i}^2/2}}{x_{3,i}\sqrt{2\pi}}}_{\phi_7} \underbrace{\frac{e^{-x_{4,i}^2/2}}{x_{4,i}\sqrt{2\pi}}}_{\phi_8}, \quad (\text{A.3})$$

where

$$\begin{aligned} c_2 &= \frac{m_w\gamma_{th2}}{\Omega_{SR}\rho_s d_w^{-\nu}}, \\ x_{3,i} &= \frac{\ln\left(\frac{\gamma_{th1}}{\rho_{Ri}(a_1(1+\gamma_{th1})-\gamma_{th1})e^{-2\theta d_{P1}}}\right) - \mu'}{\sigma'}, \\ x_{4,i} &= \frac{\ln\left(\frac{\gamma_{th2}}{\rho_{Ri}(1-a_1)e^{-2\theta d_{P2}}}\right) - \mu''}{\sigma''}. \quad (\text{A.4}) \end{aligned}$$

Using $Q'(x) = \frac{-e^{-x^2/2}}{\sqrt{2\pi}}$, we can write the partial derivative of $OP_{sys,i}$ with respect to a_1 as

$$\begin{aligned} \frac{\partial OP_{sys,i}}{\partial a_1} &= \left[\frac{c_2}{(1-a_1)^2} \right] \phi_5\phi_6\phi_7\phi_8 + \phi_5\phi_6\phi_7 \left[\frac{e^{-x_{4,i}^2/2}}{\sigma''(1-a_1)\sqrt{2\pi}} \right] \\ &- \phi_5 \left[\frac{c_2\phi_6}{(1-a_1)^2} - \frac{c_2^{m_w}}{(m_w-1)!(1-a_1)^{m_w+1}} \right] \phi_7\phi_8 \\ &+ \phi_5\phi_6 \left[\frac{e^{-x_{3,i}^2/2}}{\sigma'\sqrt{2\pi}} \times \frac{1+\gamma_{th1}}{\gamma_{th1}-a_1(1+\gamma_{th1})} \right] \phi_8 \\ &= \phi_5\phi_6\phi_7\phi_8 \times f(a_1) = (1 - OP_{sys,i}) \times f(a_1), \quad (\text{A.5}) \end{aligned}$$

where

$$\begin{aligned} f(a_1) &= \sum_{m=0}^{m_w-1} \frac{m!c_2^{m_w-m}}{(m_w-1)!(1-a_1)^{m_w+1-m}} \\ &+ \frac{x_3}{\sigma'(\frac{\gamma_{th1}}{1+\gamma_{th1}}-a_1)} + \frac{x_4}{\sigma''(1-a_1)}. \quad (\text{A.6}) \end{aligned}$$

Based on (A.5), we can't predict a monotonic trend in this interval. So to show the convexity of this function, the second derivative of $OP_{sys,i}$ with respect to a_1 must be positive. We can write the second derivative as

$$\begin{aligned} \frac{\partial^2 OP_{sys,i}}{\partial a_1^2} &= \frac{\partial f(a_1)}{\partial a_1} (1 - OP_{sys,i}) - \frac{\partial OP_{sys,i}}{\partial a_1} f(a_1), \\ &= \underbrace{(1 - OP_{sys,i})}_{\text{Always+ve}} \left[\frac{\partial f(a_1)}{\partial a_1} - f^2(a_1) \right], \quad (\text{A.7}) \end{aligned}$$

where

$$\begin{aligned} \frac{\partial f(a_1)}{\partial a_1} &= \sum_{m=0}^{m_w-1} \frac{m!(m_w+1-m)c_2^{m_w}}{(m_w-1)!(1-a_1)^{m_w+2-m}} \\ &+ \frac{\left(\frac{\gamma_{th1}}{1+\gamma_{th1}}-a_1\right)^{-2}}{\sigma'} \left(\frac{1}{\sigma'} + x_3\right) \\ &+ \frac{(1-a_1)^{-2}}{\sigma''} \left(\frac{1}{\sigma''} + x_4\right). \quad (\text{A.8}) \end{aligned}$$

After some mathematical manipulation, we can prove that $\left[\frac{\partial f(a_1)}{\partial a_1} - f^2(a_1)\right]$ in (A.7) is a positive value, which demonstrates the convexity of the proposed function in this interval.

From the analysis carried out over the two intervals of a_1 , we can conclude that the proposed optimization function in (46) is convex over the entire range of a_1 .

REFERENCES

- [1] M. I. Hamed, B. M. ElHalawany, M. M. Fouda, and A. S. Tag Eldien, "A new approach for server-based load balancing using software-defined networking," in *Proc. 8th Int. Conf. Intell. Comput. Inf. Syst.*, 2017, pp. 30–35.
- [2] S. Hashima *et al.*, "Leveraging machine-learning for D2D communications in 5G/Beyond 5G networks," *Electronics*, 10, no. 2, 2021, Art. no. 169.
- [3] M. Jani, P. Garg, and A. Gupta, "Performance analysis of a mixed cooperative PLC-VLC system for indoor communication systems," *IEEE Syst. J.*, vol. 14, no. 1, pp. 469–476, Mar. 2020.

- [4] L. Yang, X. Yan, S. Li, D. B. da Costa, and M.-S. Alouini, "Performance analysis of dual-hop mixed PLC/RF communication systems," *IEEE Syst. J.*, vol. 16, no. 2, pp. 2867–2878, Jun. 2022.
- [5] H. N. Noura, R. Melki, A. Chehab, and J. H. Fernandez, "Efficient and robust data availability solution for hybrid PLC/RF systems," *Comput. Netw.*, vol. 185, 2020, Art. no. 107675.
- [6] M. Kashaf, M. Abdallah, and N. Al-Dhahir, "Transmit power optimization for a hybrid PLC/VLC/RF communication system," *IEEE Trans. Green Commun. Netw.*, vol. 2, no. 1, pp. 234–245, Mar. 2018.
- [7] A. R. Ndjiongue, T. M. N. Ngatched, O. A. Dobre, and A. G. Armada, "VLC-based networking: Feasibility and challenges," *IEEE Netw.*, vol. 34, no. 4, pp. 158–165, Jul./Aug. 2019.
- [8] S. Aboagy, S. K. Ibrahim, T. M. N. Ngatched, A. R. Ndjiongue, and O. A. Dobre, "Design of energy efficient hybrid VLC/RF/PLC communication system for indoor networks," *IEEE Wireless Commun. Lett.*, vol. 9, no. 2, pp. 143–147, Feb. 2020.
- [9] A. Kumar, S. K. Ghorai, and A. Chaudhury, "BER performance of OFDM based hybrid PLC-VLC system," in *Proc. Int. Conf. Comput. Electron. Commun. Eng.*, 2020, pp. 1–6.
- [10] A. Majumder and J. Caffery, "Power line communication: An overview," *IEEE Potentials*, vol. 23, no. 4, pp. 4–8, Apr. 2004.
- [11] H. Meng *et al.*, "Modeling of transfer characteristics for the broadband power line communication channel," *IEEE Trans. Power Del.*, vol. 19, no. 3, pp. 1057–1064, Jul. 2004.
- [12] T. Bai *et al.*, "Fifty years of noise modeling and mitigation in power-line communications," *IEEE Commun. Surv. Tut.*, vol. 23, no. 1, pp. 41–69, Jan.–Mar. 2020.
- [13] A. Mathur, M. R. Bhatnagar, Y. Ai, and M. Cheffena, "Performance analysis of a dual-hop wireless-power line mixed cooperative system," *IEEE Access*, vol. 6, pp. 34380–34392, 2018.
- [14] O. Karakuş, E. E. Kuruoğlu, and M. A. Altınkaya, "Modelling impulsive noise in indoor powerline communication systems," *Signal Image Video Process.*, vol. 14, no. 8, pp. 1655–1661, 2020.
- [15] V. B. Balakirsky and A. J. H. Vinck, "Potential limits on powerline communication over impulsive noise channels," in *Proc. 7th Int. Symp. Power-Line Commun. Appl.*, 2003, pp. 32–36.
- [16] H. Meng, Y. L. Guan, and S. Chen, "Modeling and analysis of noise effects on broadband power-line communications," *IEEE Trans. Power Del.*, vol. 20, no. 2, pp. 630–637, Apr. 2005.
- [17] L. D. M. B. A. Dib, V. Fernandes, M. D. L. Filomeno, and M. V. Ribeiro, "Hybrid PLC/Wireless communication for smart grids and Internet of Things applications," *IEEE Internet Things J.*, vol. 5, no. 2, pp. 655–667, Apr. 2018.
- [18] O. Maraqa, A. S. Rajasekaran, S. Al-Ahmadi, H. Yanikomeroglu, and S. M. Sait, "A survey of rate-optimal power domain NOMA with enabling technologies of future wireless networks," *IEEE Commun. Surv. Tut.*, vol. 22, no. 4, pp. 2192–2235, Oct.–Dec. 2020.
- [19] B. M. ElHalawany, F. Jameel, D. B. da Costa, U. S. Dias, and K. Wu, "Performance analysis of downlink NOMA systems over κ - μ shadowed fading channels," in *IEEE Trans. Veh. Technol.*, vol. 69, no. 1, pp. 1046–1050, Jan. 2020.
- [20] B. M. Elhalawany, A. A. A. El-Banna, and K. Wu, "Physical-layer security and privacy for vehicle-to-everything," *IEEE Commun. Mag.*, vol. 57, no. 10, pp. 84–90, Oct. 2019.
- [21] S. M. R. Islam, N. Avazov, O. A. Dobre, and K. S. Kwak, "Power-domain non-orthogonal multiple access (NOMA) in 5G systems: Potentials and challenges," *IEEE Commun. Surv. Tut.*, vol. 19, no. 2, pp. 721–742, Apr.–Jun. 2017.
- [22] W. Gheth, K. M. Rabie, B. Adebisi, M. Ijaz, G. Harris, and A. Alfitouri, "Hybrid power-line/wireless communication systems for indoor applications," in *Proc. Proc. 11th Int. Symp. Commun. Syst., Netw. Digit. Signal Process.*, 2018, pp. 1–6.
- [23] Y. H. Ma, P. L. So, and E. Gunawan, "Performance analysis of OFDM systems for broadband power line communications under impulsive noise and multipath effects," *IEEE Trans. Power Del.*, vol. 20, no. 2, pp. 674–682, Apr. 2005.
- [24] L. Di Bert, P. Caldera, D. Schwingshackl, and A. M. Tonello, "On noise modeling for power line communications," in *Proc. IEEE Int. Symp. Power Line Commun. Appl.*, 2011, pp. 283–288.
- [25] M. Elsayed, A. Samir, A. A. A. El-Banna, X. Li, and B. M. Elhalawany, "When NOMA multiplexing meets symbiotic ambient backscatter communication: Outage analysis," *IEEE Trans. Veh. Technol.*, vol. 71, no. 1, pp. 1026–1031, Jan. 2022, doi: [10.1109/TVT.2021.3127043](https://doi.org/10.1109/TVT.2021.3127043).
- [26] W. U. Khan, M. A. Javed, T. N. Nguyen, S. Khan, and B. M. Elhalawany, "Energy-efficient resource allocation for 6G backscatter-enabled NOMA IoV networks," *IEEE Trans. Intell. Transp. Syst.*, to be published, doi: [10.1109/TITS.2021.3110942](https://doi.org/10.1109/TITS.2021.3110942).
- [27] W. U. Khan *et al.*, "Energy efficiency maximization for beyond 5G NOMA-enabled heterogeneous networks," *Peer-to-Peer Netw. Appl.* vol. 14, pp. 3250–3264, 2021.
- [28] B. M. ElHalawany, M. Elsabrouty, O. Muta, A. Abdelrahman, and H. Furukawa, "Joint energy-efficient single relay selection and power allocation for analog network coding with three transmission phases," *Proc. 79th Veh. Technol. Conf.*, 2014, pp. 1–7.
- [29] P. A. Shirinabadi and A. Abbasi, "On approximation of Gaussian Q-function and its applications," in *Proc. IEEE 10th Annu. Ubiquitous Comput. Electron. Mobile Commun. Conf.*, 2019, pp. 0883–0887.
- [30] S. M. Ibraheem, W. Bedawy, W. Saad, and M. Shokair, "Outage performance of NOMA-based DF relay sharing networks over Nakagami-m fading channels," in *Proc. 13th Int. Conf. Comput. Eng. Syst.*, 2019, pp. 512–517.
- [31] Z. Wang and G. B. Giannakis, "A simple and general parameterization quantifying performance in fading channels," *IEEE Trans. Commun.*, vol. 51, no. 8, pp. 1389–1398, Aug. 2003.
- [32] B. Zhu, J. Cheng, J. Yan, J. Wang, L. Wu, and Y. Wang, "A new asymptotic analysis technique for diversity receptions over correlated lognormal fading channels," in *IEEE Trans. Commun.*, vol. 66, no. 2, pp. 845–861, Feb. 2018.
- [33] D.-T. Do, M.-S. V. Nguyen, F. Jameel, R. Jäntti, and I. S. Ansari, "Performance evaluation of relay-aided CR-NOMA for beyond 5G communications," *IEEE Access*, vol. 8, pp. 134 838–134 855, 2020, doi: [10.1109/ACCESS.2020.3010842](https://doi.org/10.1109/ACCESS.2020.3010842).
- [34] A. Rauniyar, P. Engelstad, and O. N. Sterb, "Ergodic capacity performance of noma-swift aided IoT relay systems with direct link," in *Proc. 18th Int. Symp. Model. Optim. Mobile, Ad Hoc, Wireless Netw.*, 2020, pp. 1–8.
- [35] M. Abramowitz and I. A. Stegun, *Handbook of Mathematical Functions With Formulas, Graphs, and Mathematical Tables*. New York, NY, USA: Dover, 1964.
- [36] A. Dubey, D. Sharma, R. K. Mallik, and S. Mishra, "Modeling and performance analysis of a PLC system in presence of impulsive noise," in *Proc. IEEE Power Energy Soc. Gen. Meeting*, 2015, pp. 1–5.
- [37] A. Dubey, R. K. Mallik, and R. Schober, "Performance of a PLC system in impulsive noise with selection combining," in *Proc. IEEE Glob. Telecommun. Conf.*, 2012, pp. 3508–3512.
- [38] A. Laourine, M.-. Alouini, S. Affes, and A. Stephenne, "On the performance analysis of composite multipath/shadowing channels using the G-distribution," in *Proc. IEEE Int. Conf. Commun.*, 2008, pp. 1333–1338.